

# BLADE ELEMENT MOMENTUM CALCULATION METHOD WITH VARIOUS CORRECTIONS

Fike, M.; Pezdevsek, M.; Predin, A. & Hren, G.

University of Maribor, Faculty of Energy Technology, Hočevarjev trg 1, 8270 Krško, Slovenia

E-Mail: matej.fike@um.si

## Abstract

Blade element momentum theory is widely used for predicting wind turbine aerodynamic performance. Unfortunately, power and thrust coefficients predicted by momentum theory deviated dramatically from the experimental data when the value of the axial induction factor was more significant than 0.5. To solve this problem and to increase the accuracy of the prediction, correction for the high value of the axial induction factor must be applied. Using BEM theory, this paper uses analytical prediction for power output compared with different existing correction models used to improve the basic calculation of the turbine power output. The results are compared to experimental measurement results for a small wind turbine. Considering all the comparisons, we note minor differences in the results between the Modified ABS and Buhl models on the one hand and between the Spera and Wilson models on the other, that matches our measurements best.

(Received in March 2023, accepted in April 2023. This paper was with the authors 1 week for 1 revision.)

**Key Words:** BEM Method, S826 Airfoil, Horizontal Axis Wind Turbine, Aerodynamic Performance, Power Coefficient

## 1. INTRODUCTION

The importance of renewable energy in tomorrow's energy market becomes evident from the energy policies of different developed and developing nations worldwide for the next decades. Renewable energy resources like wind and solar energy have been known as the types of clean energy that have a lower impact on the environment than fossil fuels. With the rapid advancement of wind turbine technology and its expansion in the energy production portfolio of countries, the need to study and optimize the performance of wind turbines for different climatic conditions has become very important for wind energy engineers. Wind power production is expected to be a considerable part of the future energy mix.

A wind turbine is a machine that extracts kinetic energy from the wind [1]. With the development of numerical methods and computational power, computational fluid dynamics (CFD) method is widely used to research aerodynamic behaviour and flow phenomena of wind turbines with the aim of efficient utilization of wind energy. Although the CFD method has high time and computer resource requirements, it is essential in investigating and predicting wind turbine performance. Karlsen [2] used CFD simulations in Ansys Fluent to predict the power and thrust coefficients of a horizontal wind turbine and observed good agreement between experimental data and simulation results [2]. Similarly, Fike et al. [3] simulated wind turbine performance with Ansys CFX, and the results showed good agreement with experimental measurements. Czyz and Karpinski [4] used CFD simulations to examine the aerodynamic forces and moments on an X-tail stabilizer in a hybrid aircraft.

BEM theory is based on two decompositions, a radial decomposition of the blades and the fluid column, considered as concentric rings that do not interact with each other, and a decomposition of the fluid/turbine system into a visible part via Momentum Theory and a local planar part via Blade Element Theory [5].

Blade geometry and airfoil characteristics are required to calculate the performance of a wind turbine with the BEM method operational conditions. Forces that act on the blade are

described in terms of lift and drag coefficients, and they are a function of the attack angle. Airfoil characteristics, such as lift and drag coefficients, used in BEM calculations are usually obtained with 2D wind tunnel tests or CFD simulations. Fike et al. researched an airfoil's steady and unsteady static-stall aerodynamic characteristics at a low Reynolds number. Yang et al. [6] predicted wind turbine performance using BEM with airfoil data extracted from CFD.

The BEM methods are inherently much faster than numerical computation methods. They require a less computational resources but can only model limited aerodynamic phenomena on an actual turbine [1]. In BEM theory, the flow through the rotor disc is assumed to be uniform in the azimuthal direction. However, this needs to be revised for a realistic turbine with usually only three blades. Application of the classic BEM method shows bad agreement between measured and calculated values at higher axial induction values. Recently, the BEM theory has been optimized and modified to provide more accurate results.

For a high value of axial induction factor, a turbulent wake usually appears, and it is broadly considered that momentum theory does not apply. This fact was already reported by Glauert [5], who proposed some corrections. Later, researchers also work on corrections. We highlight corrections made by Wilson [7] and Spera [8], and Buhl [9]. The correction proposed by Buhl are implemented in the QBlade and NREL's AeroDyn software.

In the present work, we compared the power coefficient predicted by the blade element momentum method with six different corrections for a high value of axial induction factor with and without corrections for tip and hub losses and cascade correction. The results are compared with own experimental results for the power coefficient curve of a small model-sized wind turbine.

## **2. MATHEMATICAL MODEL**

The BEM method combines the momentum and blade element theory. The blade is divided into several sections, and by applying the equations of momentum and angular momentum conservation, axial force and torque are calculated for each section of the blade.

However, the thrust coefficient predicted by classic BEM methods does not agree with experimental data when the value of the axial induction factor is higher than 0.5 [10]. In addition, tip losses, hub losses, three-dimensional effects, and other possible calculation errors need to be considered when making corrections to the original blade element momentum theory.

### **2.1 Tip and hub losses**

Because the upwind and downwind surfaces have different adjacent air pressure, the wind will change direction at the tip and the hub, leading to an aerodynamic loss. Prandtl corrected the assumption of an infinite number of blades and derived a correction factor  $F$  to equations, including tip loss  $F_t$  and hub loss  $F_h$  [11, 12].

The tip loss factor  $F_t$  is expressed as:

$$F_t = \frac{2}{\pi} \arccos e^{-\frac{B(R-r)}{2r \sin \varphi}} \quad (1)$$

where  $B$  is the number of blades,  $R$  is tip radius,  $r$  is section radius and  $\varphi$  is angle of relative wind.

The hub loss  $F_h$  is expressed as:

$$F_h = \frac{2}{\pi} \arccos e^{-\frac{B(r-R_{hub})}{2R_{hub} \sin \varphi}} \quad (2)$$

and the total losses are expressed as:

$$F = F_t F_h \quad (3)$$

Shen et al. [13] corrected both the induced velocities and the mass flux for tip loss effects by introducing a new function,  $g$ , which generally depends on the tip speed ratio  $\lambda$  and the number of blades  $B$ , as well as the chord distribution and pitch angles [11]. Shen et al. also give a simplified function dependent only on the number of blades  $B$  and the tip speed ratio using the experimental data:

$$g = e^{-0.125(B\lambda-21)} + 0.1 \quad (4)$$

Shen's tip loss and hub loss factors now take the following form:

$$F_t = \frac{2}{\pi} \arccos e^{-g \frac{B(R-r)}{2r \sin \varphi}} \quad (5)$$

$$F_h = \frac{2}{\pi} \arccos e^{-g \frac{B(r-R_{hub})}{2R_{hub} \sin \varphi}} \quad (6)$$

where  $R_{hub}$  is hub radius.

The total Shen's loss is expressed as:

$$F = F_t F_h \quad (7)$$

## 2.2 Cascade correction

The effects of the rotor's finite width and the blade's thickness give rise to changes in the angle of attack, known as cascade effects. The greater the solidity, the more corrections are needed. The equations were obtained in [14].

Circulation change, due to the curvature of the flow, as the result of the finite chord width is given by:

$$\Delta\alpha_1 = \frac{1}{4} \left[ \tan^{-1} \frac{(1-a)V}{(1+2a')r\Omega} - \tan^{-1} \frac{(1-a)V}{r\Omega} \right] \quad (8)$$

where  $\alpha$  is angle of attack,  $V$  is wind speed and  $\Omega$  is rotational velocity.

The second cascade effect results from the thickness of the airfoil.

$$\Delta\alpha_2 = 0.109 \frac{Bct_{max}\lambda}{Rc \sqrt{(1-a)^2 + \left(\frac{r\lambda}{R}\right)^2}} \quad (9)$$

where  $t_{max}$  is the maximum thickness of the airfoil and  $c$  section chord length.

The new angle of attack is then:

$$\alpha_{cascade} = \alpha + \Delta\alpha_1 + \Delta\alpha_2 \quad (10)$$

## 2.3 Correction for high axial induction values

The stream tube theory is used in BEM calculation methods and is considered valid for small wake expansion. However, it fails for sizeable axial induction factor values when the turbine operates at high tip speed ratios. According to momentum theory, such turbine operation occurs when some of the flow in the far wake starts to propagate upstream, but this does not match the basic assumption of the BEM theory. The classic BEM theory equation  $V_4 = V_1(1 - 2a)$  is not physical for a wind turbine when the axial induction factor exceeds approximately 0.5, and the simple momentum theory fails [15]. This flow reversal is not physical and cannot occur. In reality, under such operating conditions, more flow invades from outside the wake, and the turbulence increases. Further investigations showed that measurements and BEM calculation results do not agree when the axial induction factor is over a critical value usually set between 0.2 and 0.4. Almost 100 years ago, Glauert [5] developed a correction to the rotor thrust coefficient of an entire rotor. Later several researchers continued to research this topic and developed multiple empirical models:

- Classic BEM,
- Wilson,

- Spera,
- Modified ABS,
- Buhl Correction (Aerodyn),
- Buhl Correction (QBlade).

In this section, the models mentioned earlier are described.

The classical BEM theory is described in several texts in various levels of detail, e.g., [15, 16]. When the thrust equations from momentum theory and blade element theory are equated and performed some algebraic manipulation, equations of the axial induction factor and tangential induction factor are obtained [10].

$$a = \frac{\sigma C_n}{(4F \sin^2 \varphi + \sigma C_n)} \quad (11)$$

$$a' = \frac{\sigma C_t}{(4F \sin \varphi \cos \varphi - \sigma C_t)} \quad (12)$$

where  $\sigma$  is solidity ratio,  $C_n$  is normal coefficient,  $C_t$  is tangential coefficient and  $F$  is loss factor.

In 1984 Wilson reported the Wilson and Walker method [7]. They proposed following expression for the axial induction factor:

$$a = \begin{cases} \frac{1 - \sqrt{\left(1 - \frac{C_T}{F}\right)}}{2}, & C_T \leq 0.64F \\ \frac{C_T - 4Fa_c^2}{4F(1 - 2a_c)}, & C_T > 0.64F \end{cases} \quad (13)$$

$$a' = \frac{1}{\frac{4F \sin \varphi \cos \varphi}{\sigma(C_L \sin \varphi - C_D \cos \varphi)} - 1} \quad (14)$$

where  $C_L$  is lift coefficient and  $C_D$  is drag coefficient. The value used by Wilson was  $a_c = 0.2$ . This model is derived from the first order of the Taylor series. The thrust coefficient versus axial induction factor is modelled as a straight line where  $a > a_c$ . Wilson [7] stated that this model agrees with the vortex theory and experimental data.

Spera [8] proposed this expression for the axial induction factor:

$$a = 1 + 0.5(K(1 - 2a_c)) - \sqrt{[K(1 - 2a_c) + 2]^2 + 4(Ka_c^2 - 1)} \quad (15)$$

$$K = \frac{4F \sin^2 \varphi}{\sigma C_n} \quad (16)$$

The value used by Spera was  $a_c = 0.2$ . Spera modelled the thrust coefficient versus axial induction factor as a straight-line tangent to the momentum theory parabola at the critical point  $a_c$ .

Another modification of Glauert's empirical formula is Modified ABS [10]. Equations of  $a$  and  $a'$  were defined as [17]:

$$a = \begin{cases} \frac{1 - \sqrt{\left(1 - \frac{C_T}{F}\right)}}{2}, & C_T < 0.96F \\ 0.1432 + \sqrt{\left(-0.55106 + \frac{0.6427C_T}{F}\right)}, & C_T \geq 0.96F \end{cases} \quad (17)$$

$$a' = \begin{cases} 0, & 1 + a'' < 0 \\ \frac{\sqrt{(1 + a'')} - 1}{2}, & 1 + a'' \geq 0 \end{cases} \quad (18)$$

$$a'' = \frac{4aF(1-a)}{\lambda_r^2} \quad (19)$$

where  $\lambda_r$  is local speed ratio.

AeroDyn software [18] implemented a modified version of Buhl's correction of Glauert's empirical formula [9]:

$$a = \begin{cases} \frac{18F - 20 - 3\sqrt{C_T(50 - 36F) + 12F(3F - 4)}}{36F - 50} & C_T > 0.96F \\ \left[1 + \frac{4F \sin^2 \varphi}{\sigma C_n}\right]^{-1} & C_T \leq 0.96F \end{cases} \quad (20)$$

$$a' = \left[-1 + \frac{4F \sin \varphi \cos \varphi}{\sigma C_t}\right]^{-1} \quad (21)$$

QBlade software, presented by [19], as seen in [20], uses the same model, except for calculating  $a'$ , where the following expression is used:

$$a' = \frac{1}{2} \left( \sqrt{\left|1 + \frac{4a(1-a)}{\lambda^2}\right|} - 1 \right) \quad (22)$$

## 2.4 Calculation

The calculations are performed by software written in Python that is used to predict the power output of HAWTs. The algorithm of the Blade Element Momentum Method:

1. Calculate the local velocity ratio of the section  $\lambda_r$ , the local solidity  $\sigma$ .
2. Initialize the axial induction factor  $a$  and the tangential induction factor  $a'$ , in our case we start with constant values  $a = 0.3$  and  $0.01$  for each section.
3. Calculate the normal velocity components  $v_1(1-a)$  and the tangential velocity components  $\omega r(1+a')$  and their resultants  $v_{rel}$ .
4. Based on  $v_{rel}$ , calculate the Reynolds number of the section.
5. Based on the normal and tangential components of the velocity, calculate the relative wind angle  $\varphi$ .
6. With the data collected so far, compute the losses at the tip and at the foot of the blade  $F_{tip}$  and  $F_{hub}$ .
7. With the yaw angle  $\theta$ , the pitch angle  $\Lambda$  and the relative wind angle  $\varphi$ , compute the angle of attack  $\alpha$ .
8. At this point consider any corrections due to the cascading effect.
9. Based on the angle of attack  $\alpha$ , the coefficients  $C_l$  in  $C_d$  read off from the tables.
10. Consider possible rotational augmentation corrections.
11. Compute the normal and tangential coefficient  $C_n$  in  $C_t$ .
12. With all the necessary data and according to the needs of the given method, compute the axial induction coefficient  $a$ , the angular induction coefficient  $a'$  and the local thrust factor  $C_{T_r}$ .
13. Compute all the other forces of the given section  $dF_l$ ,  $dF_d$ ,  $dF_n$ ,  $dF_t$  and the total incremental torque and thrust  $dM$  in  $dT$ .
14. Check convergence based on the difference between the axial induction factor in the previous iteration and in the current iteration. If convergence is achieved, proceed to step 16, otherwise proceed to step 15.
15. If convergence is not achieved, the possible relaxation factor is taken into account, the old value of the axial and tangential induction factor is saved and the process is repeated from step 3.
16. If convergence is achieved, save the data of the given section and continue.

17. After collecting the calculation results for all sections, the total thrust, torque, power and efficiency is calculated.

The outline of the calculation process is presented in Fig. 1.

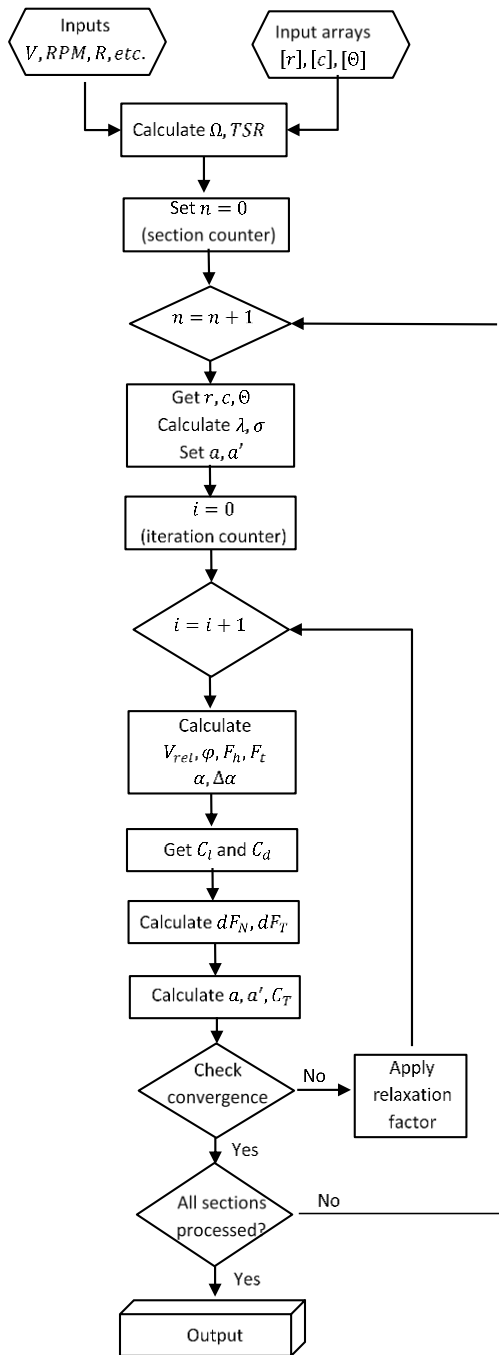


Figure 1: Calculation algorithm.

In the lack of experimental data for the lift and drag coefficients, results from XFOIL [21] were used as input for calculations and comparison with measurement data.

It is important to note that the local thrust coefficient  $C_T$  value is calculated using the equation:

$$C_T = \frac{dF_N}{\frac{1}{2}\rho V^2 \pi r dr} = \frac{\sigma(1-a)^2 C_n}{\sin^2 \varphi} \quad (23)$$

and we have implemented an optional relaxation factor:

$$a = a_{previous} + f_r(a - a_{previous}) \quad (24)$$

where  $f_r$  is the relaxation factor. If  $f_r = 1$ , there is no change in the value of the induction factor, which is going to be used in the next iteration. Normal practice is to set  $f_r < 1$ , which dampens the iteration oscillation, thus increasing stability, but also increasing the number of iterations needed for the solution to converge. In our calculation, it was set to 0.3. Due to the very low Reynolds number range, it was necessary to consider boundary layer transition. Lift and drag coefficients were calculated using XFOIL equations at  $N_{crit.} = 9$ . This value is recommended for standard simulations of wind tunnel operation [22].

## 2.5 Geometry

The horizontal axes wind turbine examined in this paper has been developed for testing in the Laboratory for Aero and Hydro Energy Technology, which is a part of the Institute of Energy Technology at the University of Maribor. The wind turbine consists of three blades. The initial shape of the blade was taken from [2] with a tip radius of 0.45 m and an S826 airfoil. Due to the 3D printer height limitation, the original blade was scaled by a factor of 0.74. A new blade hub was also modelled. The diameter of the rotor was 0.63 m. The blade is shown in Fig. 2.

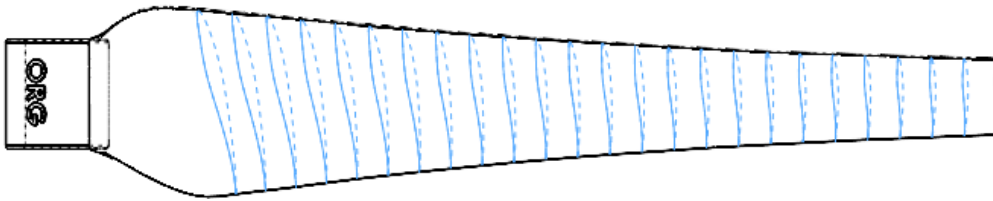


Figure 2: Wind turbine blade.

## 2.6 Measurement data

Wind turbine power coefficient characteristics were measured in a closed loop wind tunnel. The wind tunnel has a test cross-section of  $2 \text{ m} \times 2 \text{ m}$  and is powered by a 160 kW fan. Measurements were performed at the wind speed of 5.2 m/s. Inflow velocity was determined with 2D LDA system 2D FLX 500 FlowExplorer placed on a lightweight traverse system. The wind turbine rotor was attached to the electromotor and regulated with a frequency converter to control the rotational speed of the wind turbine. The electric motor was floating on a stand. A lever was attached to the motor housing, which prevented rotation around its axis via force sensor HBM U9C 200N. Measurements were done with varying rotational speeds of the wind turbine, keeping all other parameters constant. The largest uncertainty of the power coefficient measurements may be taken as 10 %, especially in the wind turbine operating conditions where the local angle of attack is increasing over the blade indicating, that the dynamic effects are related to flow separation.

## 3. RESULTS AND DISCUSSION

Fig. 3 shows the local thrust coefficient versus the axial induction factor. When the axial induction factor is lower than 0.2, the calculated thrust coefficient is the same for all methods used. Above this value, the Spera and Wilson models begin to differ from the rest, giving similar results. The course of the thrust coefficient in both models is almost linear. They differ only in the slope, which is more significant in the case of the Spera model. It can be seen from the figure that the Buhl Aerodyn and Modified ABS models predict almost the same local thrust coefficients for the given  $a$ . The mentioned models differ slightly from each other in the range of  $0.35 < a < 0.45$ . The Classic BEM method predicts a parabolic course of the thrust coefficient,

which does not follow the phenomenon's physics. That was also the primary reason for the development of new correction models.

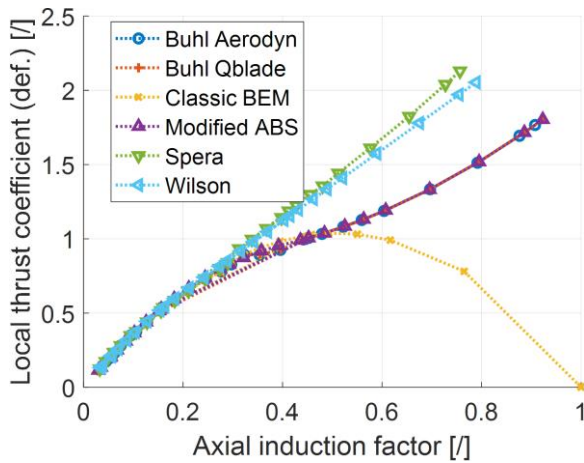


Figure 3: Local thrust coefficient versus axial induction factor.

Fig. 4 presents the axial induction factor versus section radius for three tip speed ratios. At small tip speed ratios ( $TSR$ ) numbers, the values of  $a$  are low and are smaller than the critical  $a_c$ , which in some models is 0.2. The differences between individual models are minimal and decrease as they move toward the top of the blade. At optimal  $TSR$ , the values of the blade's lower and middle parts are almost the same for different models. Approaching the tip of the blade, the differences between the models increase. The most significant differences can be seen at the tip of the blade. The Classic BEM, Modified ABS and both Buhl models predict higher  $a$  values compared to the Spera and Wilson models. At higher  $TSR$  values, the differences between the models increase by approaching the tip of the blade. Unlike the optimal  $TSR$ , the results of the classic BEM method towards the tip of the blade no longer match the Modified ABS and both Buhl models.

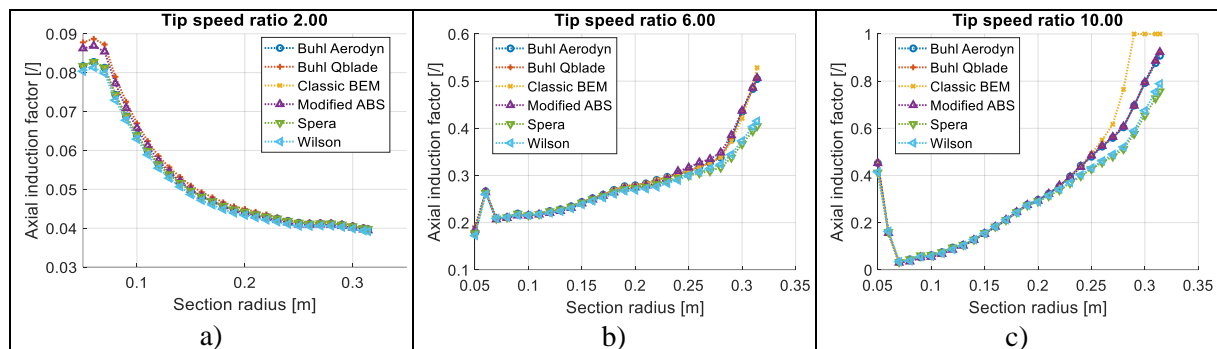


Figure 4: Axial induction factor versus section radius for three different tip speed ratios.

The number of iterations required for various correction are presented in Fig. 5. The number of iterations required increases from the hub to the tip of the blade and increased with increasing  $TSR$  number. Computationally, the Classic BEM method is the most demanding. The following is the Spera correction method. The methods with the remaining corrections do not differ significantly in the number of iterations versus section radius.

Firstly, comparing a rotor power coefficient curve predicted by the classic BEM theory without any correction model to the measured rotor power coefficient curve is convenient. Considering the first part, where the tip speed ratio is smaller than 5 in Fig. 6, the predicted curve deviated from the measured one. In the second part ( $5 < TSR < 10$ ), the predicted power coefficient is less than the measured data.

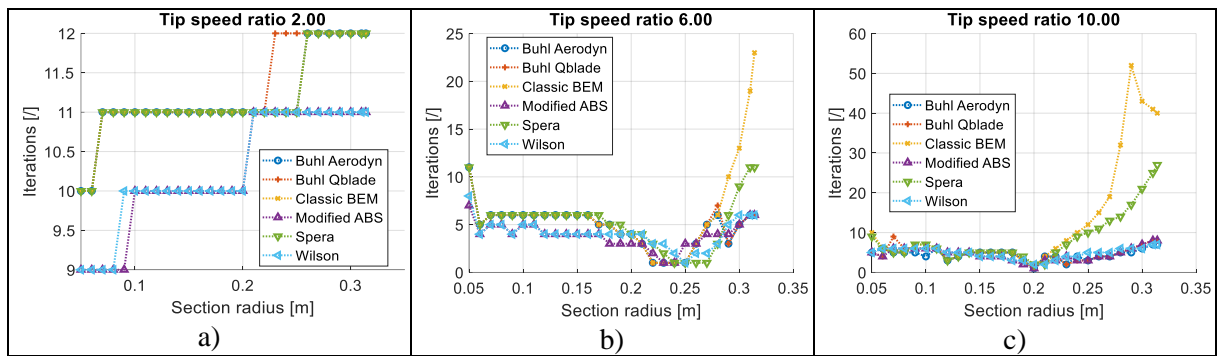


Figure 5: Number of iterations required for various corrections for three different tip speed ratios.

Secondly, all predicted power coefficient curves with correction for the high value of induction factor are compared to the classic BEM method using no correction model for high values of axial induction factor. Again, the whole diagram can be divided into two parts. The first part shows an excellent agreement of all correction models with the classic BEM model. In the second part, the results differ. The Modified ABS and Buhl models still go well with the Classic BEM model. However, we can see a slight increase in the mentioned models from the Classic BEM with an increase in the  $TSR$ , especially in the  $TSR > 8$  range.

Spera and Wilson models in the  $TSR > 5$  range predict higher power coefficients than the Classic BEM model. The differences between the two mentioned models are minimal.

Furthermore, all predicted power coefficient curves with correction for the high value of induction factor are compared to the measurement data. In the range  $TSR < 5$ , all models predict higher values of the power coefficient than were measured. Near  $TSR = 5$  the predicted power curves intersect the measured values curve, and from here on, all models underpredict the power coefficient.

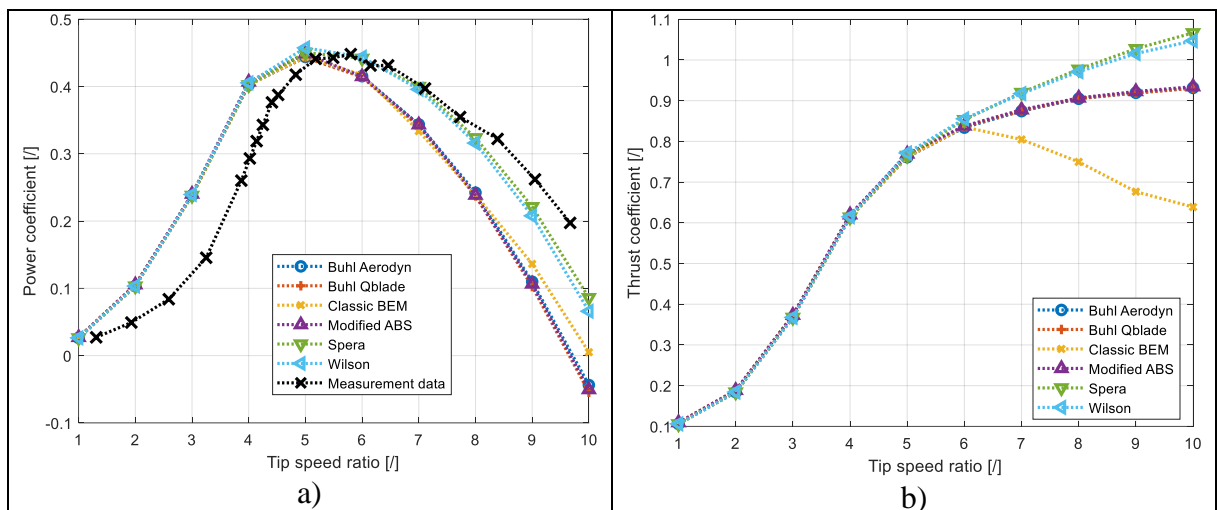


Figure 6: Power coefficient (a) and thrust coefficient (b) versus Tip speed ratio.

Similar observations apply to the course of the thrust coefficient and the course of the power coefficient. In the range of  $TSR$  from 1 to 5, all models, including the Classic BEM, predict the same course of the thrust coefficient. Differences occur in the range of  $TSR > 5$ . In the Classic BEM method, the thrust coefficient increases up to the value  $TSR = 5$ , after which the value starts to decrease parabolically. The Modified ABS model and both Buhl models predict the same course of the thrust coefficient. Spera and Wilson's model models differ slightly in their prediction. Both models predict an increase in thrust coefficient as a function of  $TSR$ , with the Spera model predicting a slightly higher value compared to the Wilson model.

A comparison of all models was performed, considering the correction for the hub, blade tip losses, and cascade losses (Fig. 7). The Shen model was considered to calculate the losses at the hub and tip of the blade. The equations described in chapter 3.2 were used to calculate cascade losses. The range of  $TSR < 4$  the power coefficient prediction of all models is not significantly different from the models without considering the corrections for losses at the hub, tip of the blade and cascade losses. In the range  $TSR > 4$ , the impact of losses increases with increasing  $TSR$ . Taking into account the mentioned losses cause a difference in the results between the models of both Buhl models (Buhl Aerodyne and Buhl QBlade) and the Modified ABS model.

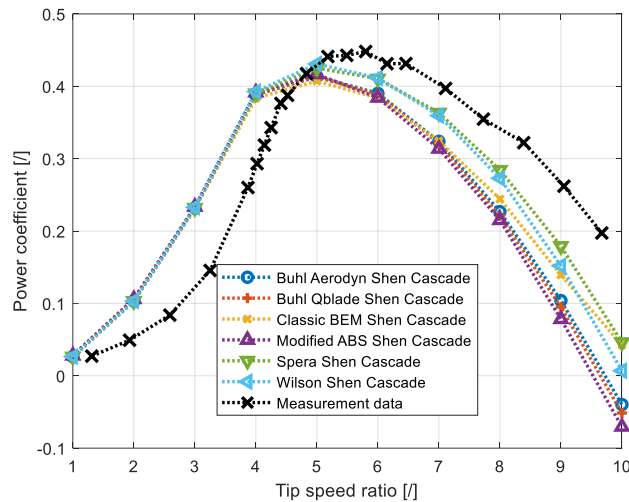


Figure 7: Power coefficient versus tip speed ratio for models with included correction for hub, tip and cascade losses.

The predicted and measured power coefficients were compared with the coefficient of determination, and calculated values are shown in Table I.

Table I: Calculated coefficient of determination for various correction model without and with hub, tip and cascade losses.

Correction model	$R^2$	Correction model	$R^2$
Buhl Aerodyn	0.585	Buhl Aerodyn Shen Cascade	0.570
Buhl Qblade	0.565	Buhl Qblade Shen Cascade	0.544
Classic BEM	0.626	Classic BEM Shen Cascade	0.665
Modified ABS	0.570	Modified ABS Shen Cascade	0.511
Spera	0.825	Spera Shen Cascade	0.746
Wilson	0.794	Wilson Shen Cascade	0.686

If we compare Fig. 6 a and Fig. 7, we find that considering the corrections, all models' power coefficient curves in the working range decrease. The calculation of the coefficient of determination shows that the best method, when corrections are not considered, is the Spera method, followed by the Wilson method. Interestingly, the agreement with the measurement results is better with the Classic BEM method, which does not consider the corrections for the high value of axial induction factor, than with both Buhl corrections (Aerodyne and Qblade) and Modified ABS. A similar conclusion applies to the models considering the hub, tip, and cascade losses. The difference is that the Modified ABS and Buhl Qblade models switched the rank determined by the coefficient of determination.

## **4. CONCLUSION**

Based on BEM theory, this paper describes the comparison of the wind turbine results predicted by using six different high values of axial induction factor correction models with each other to the measured power coefficient curve of the small model-size wind turbine.

The main findings are:

- As the  $TSR$  increases, the differences between the models in the axial induction factor increase.
- As the  $TSR$  increases, the number of required iterations increases. All models for the high value of induction factor are less computationally demanding than the classic BEM method.
- Considering all the comparisons made, we note minor differences in the results between the Modified ABS and Buhl models on the one hand and between the Spera and Wilson models on the other.

The Spera model matches our measurements best, followed by the Wilson model.

On the other hand, we observe different deviations in the course of the power coefficient in the models. If we consider corrections for hub, tip, and cascade losses, the deviation increases even more. The reasons for this deviation may be as follows:

- Incorrect value of lift and drag coefficient used in the calculation. Studies have shown that XFOIL predicts lift and drag coefficient quite accurately, but at a low Reynolds number the deviations are significant [23].
- The airfoil efficiency is reduced at a low Reynolds number, regardless of the transition criteria. Reducing the Reynolds number implies that viscous effects become more dominating, increasing viscous drag. The thickness of the boundary layer will increase with decreasing Reynolds number, leading to increased form drag or less lift [24].
- High value of  $N_{crit}$  number. According to a study [2], the  $N_{crit} = 9$  is too conservative for the conditions in the wind tunnel. That shows that the laminar flow effects predicted by XFOIL in the two-dimensional study are not present in the experiment for the Reynolds numbers in question.

## **REFERENCES**

- [1] Guntur, S. (2013). *A Detailed Study of the Rotational Augmentation and Dynamic Stall Phenomena for Wind Turbines*, DTU Wind Energy PhD No. 0022, Danmarks Tekniske Universitet, Roskilde
- [2] Karlsen, J. A. (2009). *Performance Calculations for a Model Turbine*, Master Thesis, Norwegian University of Science and Technology, Trondheim
- [3] Fike, M.; Pezdevšek, M.; Hren, G. (2015). Numerical performance calculations for a model wind turbine, *Proceedings – Zbornik del, Kuhljevi dnevi 2015*, 41-48 (in Slovenian)
- [4] Czyz, Z.; Karpinski, P. (2020). Aerodynamic characteristics of the X-tail stabilizer in a hybrid unmanned aircraft, *International Journal of Simulation Modelling*, Vol. 19, No. 4, 631-642, doi:10.2507/IJSIMM19-4-534
- [5] Glauert, H. (1926). *The Analysis of Experimental Results in the Windmill Brake and Vortex Ring States of an Airscrew*, Her Majesty's Stationery Office, London
- [6] Yang, H.; Shen, W.; Xu, H.; Hong, Z.; Liu, C. (2014). Prediction of the wind turbine performance by using BEM with airfoil data extracted from CFD, *Renewable Energy*, Vol. 70, 107-115, doi:10.1016/j.renene.2014.05.002
- [7] Wilson, R. E. (1994). Wind turbine aerodynamics Part A: Basic principles, Spera, D. A. (Ed.), *Wind Turbine Technology: Fundamental Concepts of Wind Turbine Engineering*, ASME Press, New York, 70 pages
- [8] Spera, D. A. (1994). Introduction to modern wind turbines, Spera, D. A. (Ed.), *Wind Turbine Technology: Fundamental Concepts of Wind Turbine Engineering*, ASME Press, New York, 57 pages

- [9] Buhl, M. L. Jr. (2005). *A New Empirical Relationship between Thrust Coefficient and Induction Factor for the Turbulent Windmill State*, Technical Report NREL/TP-500-36834, National Renewable Energy Laboratory, Golden
- [10] Pratumnopharat, P.; Leung, P. S. (2011). Validation of various windmill brake state models used by blade element momentum calculation, *Renewable Energy*, Vol. 36, No. 11, 3222-3227, doi:[10.1016/j.renene.2011.03.027](https://doi.org/10.1016/j.renene.2011.03.027)
- [11] Zhang, C.; Chen, H.-P. (2017). Aerodynamic performance and fatigue damage assessment of wind turbine composite blades using corrected BEM method, *Proceedings of the 8<sup>th</sup> International Conference on Structural Health Monitoring of Intelligent Infrastructure (SHMII 2017)*, 1357-1371
- [12] Prandtl, L. (1923). *Applications of Modern Hydrodynamics to Aeronautics*, NACA Technical Report No. 116, Washington, D.C.
- [13] Shen, W. Z.; Mikkelsen, R.; Sørensen, J. N.; Bak, C. (2005). Tip loss corrections for wind turbine computations, *Wind Energy*, Vol. 8, No. 4, 457-475, doi:[10.1002/we.153](https://doi.org/10.1002/we.153)
- [14] Ross Harman, C. (1994). *PROPX: Definitions, Derivations and Data Flow*, Department of Mechanical Engineering, Oregon State University, Corvallis
- [15] Hansen, M. O. L. (2008). *Aerodynamics of Wind Turbines*, 2<sup>nd</sup> ed., Earthscan – Taylor & Francis, New York
- [16] Branlard, E. (2017). *Wind Turbine Aerodynamics and Vorticity-Based Methods*, Book Series: Research Topics in Wind Energy (Vol. 7), Springer, Cham
- [17] Pratumnopharat, P.; Leung, P. S. (2016). Windmill brake state models used in predicting wind turbine performance, Lehr, J. H.; Keeley, J.; Kingery, T. B. (Eds.), *Alternative Energy and Shale Gas Encyclopedia*, John Wiley & Sons, Hoboken, 116-119, doi:[10.1002/9781119066354.ch10](https://doi.org/10.1002/9781119066354.ch10)
- [18] Moriarty, P. J.; Hansen, A. C. (2005). *AeroDyn Theory Manual*, Technical Report NREL/TP-500-36881, National Renewable Energy Laboratory, Golden
- [19] Marten, D.; Wendler, J. (2013). QBlade Guidelines, Q-Blade.Org, from [http://q-blade.org/project\\_images/files/guidelines\\_v06.pdf](http://q-blade.org/project_images/files/guidelines_v06.pdf), accessed on 22-03-2023
- [20] Marten, D.; Wendler, J. (2018). QBlade Source Code, from [https://qblade.org/downloads/#Source\\_Code](https://qblade.org/downloads/#Source_Code), accessed on 22-03-2023
- [21] Drela, M. (1989). XFOIL: An analysis and design system for low Reynolds number airfoils, Mueller, T. J. (Ed.), *Low Reynolds Number Aerodynamics*, Lecture Notes in Engineering, Vol. 54, Springer, Berlin, 1-12
- [22] Stępień, M.; Kulak, M.; Józwiak, K. (2020). “Fast Track” analysis of small wind turbine blade performance, *Energies*, Vol. 13, No. 21, Paper 5767, 16 pages, doi:[10.3390/en13215767](https://doi.org/10.3390/en13215767)
- [23] Traub, L. W.; Cooper, E. (2008). Experimental investigation of pressure measurement and airfoil characteristics at low Reynolds numbers, *Journal of Aircraft*, Vol. 45, No. 4, 1322-1333, doi:[10.2514/1.34769](https://doi.org/10.2514/1.34769)
- [24] Singh, R. K.; Ahmed, M. R.; Zullah, M. A.; Lee, Y.-H. (2012). Design of a low Reynolds number airfoil for small horizontal axis wind turbines, *Renewable Energy*, Vol. 42, 66-76, doi:[10.1016/j.renene.2011.09.014](https://doi.org/10.1016/j.renene.2011.09.014)